minerals

Article

Petrogenesis of the Late Jurassic Granodiorite and Its Implications for Tectonomagmatic Evolution in the Nuocang District, Western Gangdeses

Junsheng Jiang [1,2], Shunbao Gao [3], Bo Bao [1,*], Peng Hu [1], Xin Chen [3], Kan Tian [4], Pengcheng Huang [3], Jian Huang [3] and Xinran Guo [5]

1 Wuhan Center, China Geological Survey (Central South China Innovation Center for Geosciences), Wuhan 430205, China
2 Key Laboratory of Metallogenic Prediction of Nonferrous Metals and Geological Environment Monitoring (Central South University), Ministry of Education, Changsha 410012, China
3 Institute of Geological Survey, China University of Geosciences, Wuhan 430074, China
4 Department of Urban and Rural Planning and Architectural Engineering, Guiyang University, Guiyang 550005, China
5 The Geological Science Education Center of Guangdong, Guangzhou 510000, China
* Correspondence: baobo@mail.cgs.gov.cn

Abstract: The Gangdese magmatic rocks of the southern Lhasa terrane, are generally thought to be an important window to witness the formation and evolution of the Neo-Tethys oceanic opening, subduction, and closure, and India-Eurasian continental collision. We investigated a new occurrence of granodiorite in the Nuocang district of western Gangdese, southern Lhasa terrane, and conducted a series of analyses on their petrology, chronology, and geochemistry. The Nuocang granodiorites have the zircon U-Pb ages of 151–154 Ma, which suggest that Late Jurassic granitoids are present in the western Gangdese of southern Lhasa terrane. They are relatively high in SiO_2, Al_2O_3, low K_2O, Na_2O, and Sr/Y ratios, enrichments of LILE and LREE, and depletion of HFSE, with the positive correlation between Rb and Th, and negative correlations between SiO_2 and P_2O_5, Rb, and Y, showing the features of I-type granites. The relatively high $(^{87}Sr/^{86}Sr)_i$ values from 0.712231 to 0.712619, low εNd(t) values from −9.56 to −8.99, together with the negative εHf(t) values from −10.8 to −5.0 (mean value −8.9) suggested that the Nuocang granodiorites probably sourced from the partial melting of the ancient Lhasa terrane, with parts of mantle materials involving in. Combined with the previous geochronology and geochemical data of Mesozoic magmas in the Gangdese belt, as well as the Late Jurassic granodiorite, in this paper, we propose that the Nuocang granodiorites formed in a continental margin arc environment triggered by the northward subduction of Neo−Tethys oceanic crust.

Keywords: Nuocang granodiorites; Late Jurassic magmatism; northward subduction of Neo-Tethys oceanic crust; western Gangdese; Tibet

Citation: Jiang, J.; Gao, S.; Bao, B.; Hu, P.; Chen, X.; Tian, K.; Huang, P.; Huang, J.; Guo, X. Petrogenesis of the Late Jurassic Granodiorite and Its Implications for Tectonomagmatic Evolution in the Nuocang District, Western Gangdeses. *Minerals* **2022**, *12*, 1058. https://doi.org/10.3390/min12081058

Academic Editor: Jaroslav Dostal

Received: 2 August 2022
Accepted: 15 August 2022
Published: 21 August 2022

1. Introduction

The Lhasa terrane, as an important part of the Qinghai-Tibet Plateau, is distributed between the Bangong-Nujiang and Yarlung-Zangbo suture zones (Figure 1). Since the Mesozoic period, it has undergone a complex geological process, including the southward subduction of the Bangong-Nujiang oceanic lithosphere, the collision of the Lhasa and Qiangtang terrane, the northward subduction of the Neo-Tethys Ocean, and the continental collision of India and Eurasia, which formed a unique geological landscape in the world [1–4]. The Gangdese magmatic belt within the southern Lhasa terrane was mainly composed of large areas of Gangdese batholith and comagmatic volcanic rocks. So far, numerous researchers have conducted a series of detailed investigations on the petrogenesis and the tectonic evolution of the Cretaceous-Tertiary intrusions within the Gangdese magmatic belt and arrived at a consensus that the Neo-Tethys oceanic crust has subducted northward in Cretaceous, and take the continental collision of India and Eurasia in Paleocene [5–9]. While there are only a few pre-Cretaceous magmatic rocks occurring in the Gangdese belt [10–14], their petrogenesis and tectonic setting are still under debate. Some researchers argued that the pre-Cretaceous magmatic rocks in the Gangdese belt can be correlated with the southward subduction of the Bangong-Nujiang oceanic crust [4,15,16], while others suggested that they are the products of the northward subduction of Neo-Tethys oceanic crust [11,14,17,18]. Most of these pre-Cretaceous magmatic rocks discovered in the Gangdese belt show affinity with the growth and reworking of the juvenile crust [1,5,17,19]. In recent years, the ancient Lhasa crust has also been identified in some areas within the Gangdese belt of southern Lhasa terrane [20,21]. Thus, whether the magmatic source of pre-Cretaceous magmatic rocks in the Gangdese belt contains the ancient Lhasa crust components is still unclear.

In this study, we first discovered the Late Jurassic granodiorite in the Nuocang district of western Gangdese, southern Lhasa terrane. We present U-Pb zircon ages, Sr-Nd-Hf isotopic composition, as well as mineralogical and whole-rock geochemical data on the Nuocang Jurassic granodiorites in order to reveal the petrogenesis, tectonic evolution, and geodynamic model during Late Jurassic in western Gangdese of southern Lhasa terrane.

2. Geological Background

The Tibet plateau, the highest plateau in the world, is composed of the Songpan-Ganze, Qangtang, Lhasa, and Tethyan Himalaya terranes bounded by the Jinsha, Bangong-Nujiang, and Yarlung-Zangbo suture zones from north to south (Figure 1a, [22]). The Lhasa Terrane, separated by the Shiquanhe-Namtso Mélange Zone (SNMZ) and the Luobadu-Milashan Fault (LMF), is divided into three parts of northern, central, and southern terranes (Figure 1b; [4]). The southern and northern Lhasa terranes are generally thought to be the accreting terranes with juvenile crust, which were triggered by the northward subduction of the Neo-Tethys oceanic crust and the northward subduction of the Bangong-Nujiang oceanic crust, whereas the central Lhasa is composed of Archean-Proterozoic Nyainqentanglha basement rocks [4].

Magmatic activity widely developed in the southern Lhasa terrane, which consists of the famous Gangdese magmatic belt. It is dominantly comprised of voluminous Late Cretaceous-Tertiary Gangdese batholith (103–80 Ma; 65–40 Ma; [5]), Paleocene−Eocene Linzizong volcanic rocks (65–45 Ma; [27,28]), and Oligocene-Miocene granitoids (33–13 Ma; [29,30]). Additionally, the Early Mesozoic granitoids (205–152 Ma; [31]), and the volcanic rocks of the Early Jurassic Yeba Formation and the Late Jurassic-Early Cretaceous Sangri Group [12,32], are sporadically distributed in the southern Lhasa terrane. The central Lhasa terrane is generally thought to represent a microcontinent that experienced multi-metamorphic events during the Neoproterozoic. The overlying strata include Carboniferous-Permian and Upper Jurassic−Lower Cretaceous sedimentary rocks, with large numbers of acidic volcanic rocks and Late Triassic-early Cretaceous granitoids that are distributed near the Luobadui-Milashan Fault. The northern Lhasa subterrane is characterized by juvenile crust, with the overlying Middle Triassic to Cretaceous sedimentary rocks and an abundance of early Cretaceous medium-K calc-alkaline arc volcanic rocks and granitoids (Figure 1c).

As described above, the Mid-Late Jurassic intrusions predominantly developed in the central terrane (e.g., Xurucuo, Xiongba, Jiangba, Yangxiongle, Xiadingle, Wenbu, and Cuoqin areas; [7,16,23,33,34] and northern Lhasa terrane (e.g., Chayu, Ranwu, Sama, Bange areas; [1,34,35]). The Nuocang granodiorite in this paper is distributed in the western part of the Gangdese magmatic belt, which is firstly described in the southern Lhasa terrane. The Nuocang granodiorite was traditionally thought to be formed in the Eocene and coexisted with the Lizizong volcanic rocks of the Pana Formation [36]. In this study, we provided U-Pb ages of zircons from the Nuocang granodiorite samples and determined it was the product of Late Jurassic magmatism. It is exposed on the northern side of the Nuocang deposit, with an irregular-elliptical shape and an area of about 0.5 km^2. They intruded on the siltstone and sandstone of the early Permian Angjie Formation (Figure 2).

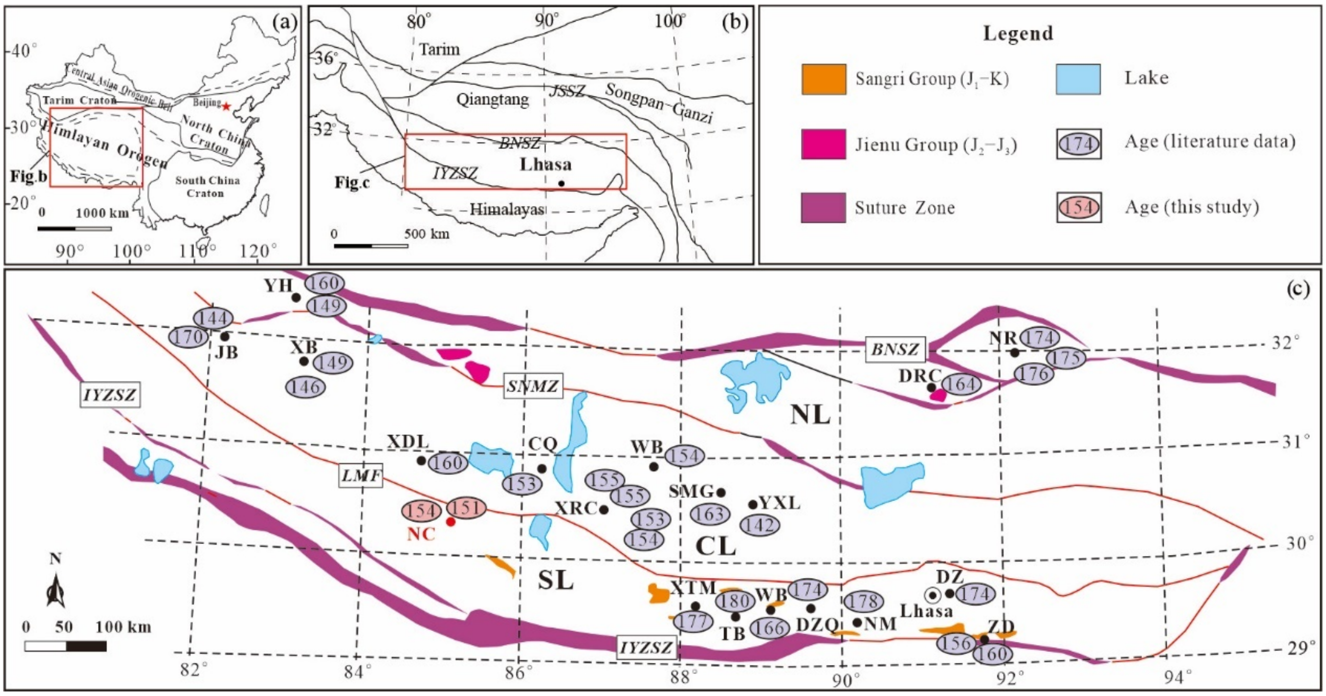

Figure 1. (**a**) Simplified structural map of China; (**b**) tectonic framework of the Himalayan-Tibetan plateau; (**c**) Simplified geologic map of the Lhasa terrane showing the major tectonic subdivisions, distribution of Mid-Late Jurassic granitoids [4,5,7,11,16,23–26] and position of the study area [4]. IYZSZ—Indus-Yarlung Zangbo Suture Zone; LMF—Luobadui-Milashan Fault; GLZCF−Gar-Lunggar−ZhariNam Tso−Comai Fault; SNMZ—Shiquan River-Nam Tso Mélange Zone; BNSZ—Bangong-Nujiang Suture Zone; NL—northern Lhasa terrane; CL—central Lhasa terrane; SL—southern Lhasa terrane; NC—Nuocang granodiorite in this study; XDL—Xiadingle intrusion; CQ—Cuoqin intrusion; JB—Jiangba intrusion; YH—Yanhu rhyolite; XB—Xiongba intrusion; XRC—Xurucuo intrusion; WB—Wenbu intrusion; SMG—Songmuguo intrusion; YXL—Yangxionglel intrusion; XTM—Xietongmen intrusion; TB—Tanabai intrusion; WB—Wobu intrusion; DZQ—Dazhuqu intrusion; NM—Nymo intrusion; DZ—Dazi intrusion; ZD—Zedong intrusion.

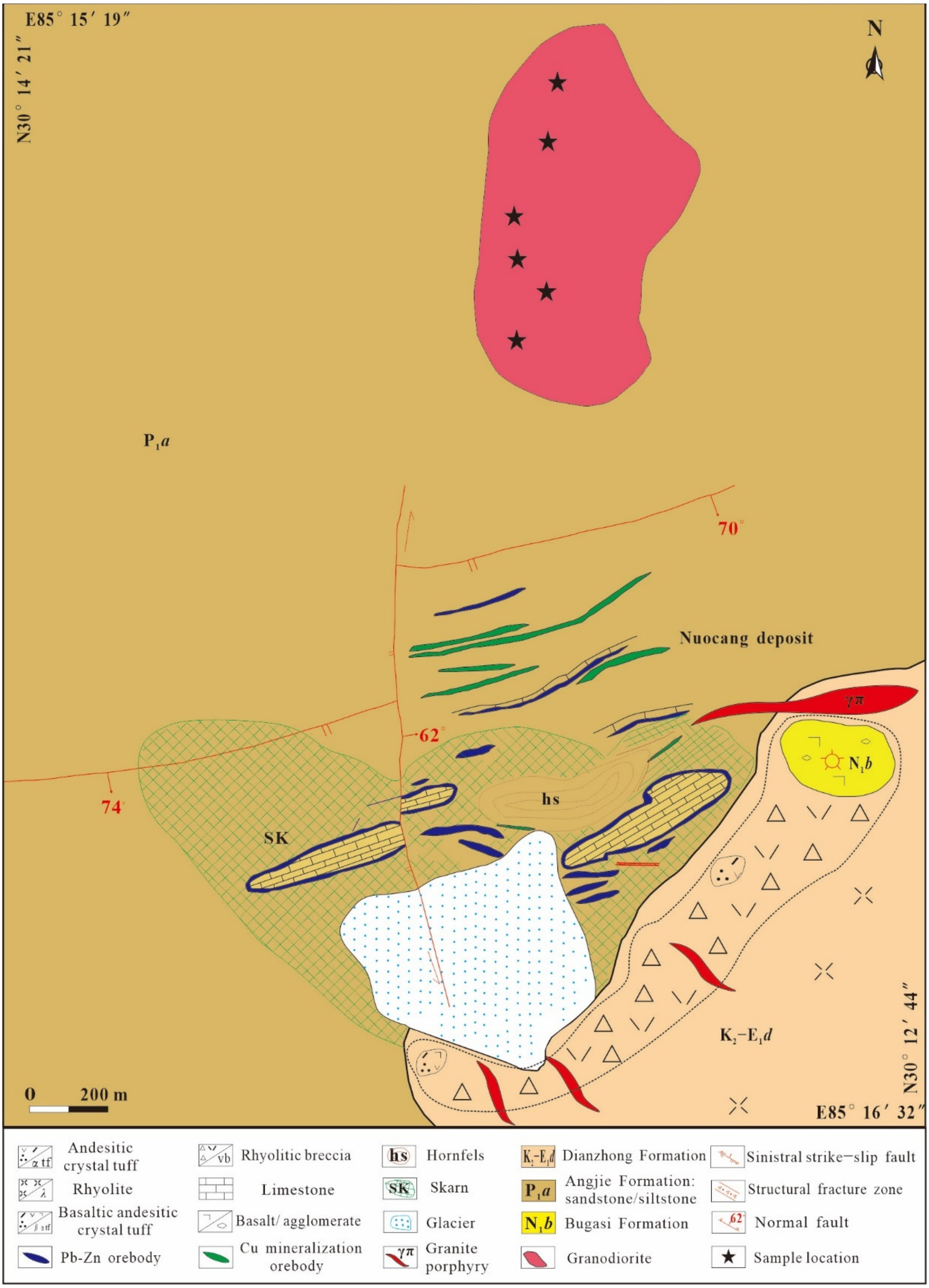

Figure 2. Simplified geological map of the Nuocang district, southern Lhasa terrane (modified after [36]).

3. Sampling and Petrography

Six samples of granodiorites were collected from the Nuocang district. The granodiorites, occurring as the stock in this district, are grey-white, with a fine-grained granitic texture (Figure 3a,b). They are composed of plagioclase (55 vol%, 0.5–4 mm), K-feldspar (7 vol%, 0.5–2 mm), quartz (18 vol%, 0.3–2 mm), amphibole (12 vol%, 0.5–1.5 mm), and biotite (7 vol%, 0.5–1.5 mm), with small amounts of zircon, monazite, apatite, and titanite (Figure 3c).

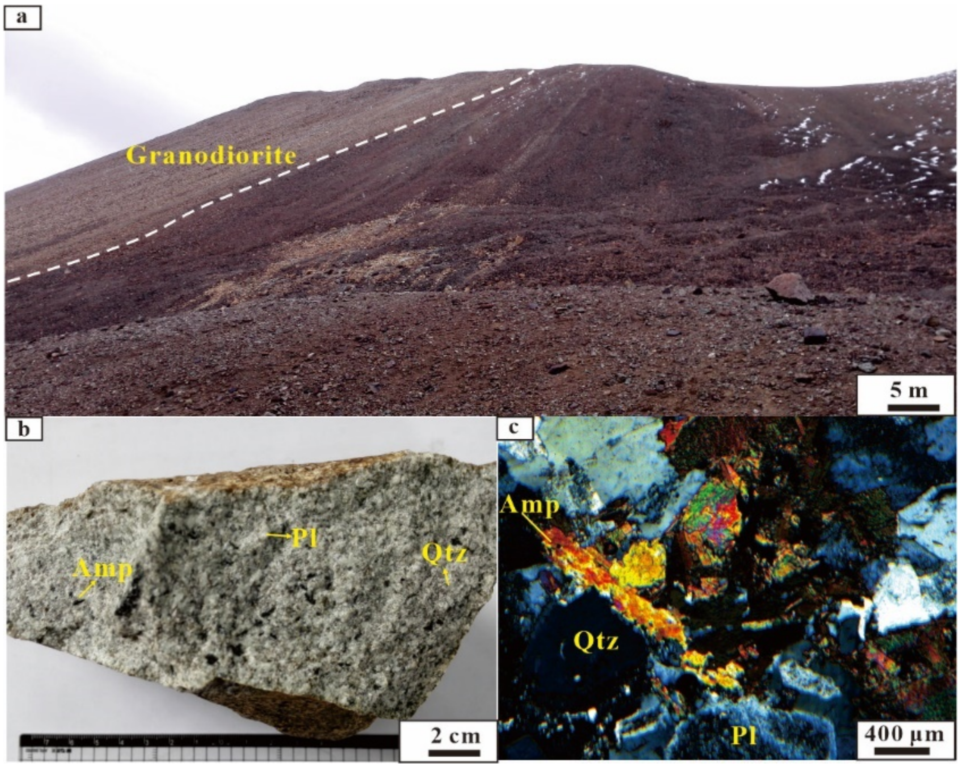

Figure 3. Outcrop photograph (**a**), typical hand specimen photographs (**b**), and microphotographs (**c**) of Nuocang granodiorite. Amp—amphibole; Pl—plagioclase; Qtz—quartz.

4. Analytical Methods

4.1. Zircon U–Pb Dating and Lu-Hf Isotopic Analyses

Before the U-Pb dating, zircon grains were polished for the purpose of showing the crystal's shape, and their internal structure was studied by transmitted and reflected light microscopy and cathodoluminescence. Zircon grains of the Nuocang granodiorites (NCNYT3 and NCNYT5) are colorless with few inclusions and exhibit oscillatory zoning (Figure 4). U-Pb dating and trace element analyses of zircon were simultaneously conducted on the LA-ICP-MS at the Wuhan Sample Solution Analytical Technology Co., Ltd. Laser sampling was performed on a GeoLasPro laser ablation system (Coherent, Santa Clara, CA, USA), and ion-signal intensities were used by an Agilent 7700e ICP-MS instrument (Agilent, Santa Clara, USA) to acquire. Sample mounts were carried by Helium, and Argon was mixed by a T-connector before entering the ICP. Zircon 91,500 and glass NIST610 were used as external standards for U-Pb dating and trace element calibration, respectively. ICPMSDataCal (10.1, Yongsheng Liu, Wuhan, China) was used to calculate for trace element analysis and U-Pb dating [37]. The age diagrams and their calculations were used by the ISOPLOT [38].

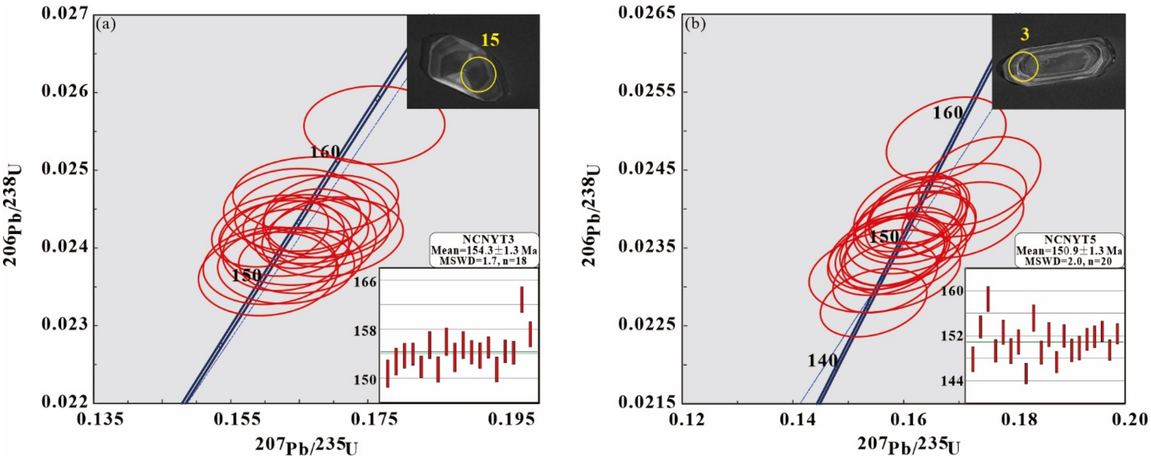

Figure 4. LA-ICP-MS U-Pb concordia diagrams and weighted mean ages for the Nuocang granodiorite samples NCNYT3 (**a**) and NCNYT5 (**b**). The insets show typical CL images of zircon grains with $^{238}U/^{206}Pb$ ages. The white scale bar in the CL images is 100 μm.

Hf isotopic analyses were conducted on a Neptune Plus MC-ICP-MS in combination with a Geolas HD excimer ArF laser ablation system in the Wuhan Sample Solution Analytical Technology Co., Ltd. The $^{179}Hf/^{177}Hf$ and $^{173}Yb/^{171}Yb$ ratios normalized to 0.7325 and 1.132685 [39] in order to calculate the mass bias of Hf (β_{Hf}) and Yb (β_{Yb}). $^{176}Lu/^{175}Lu$ = 0.02656 and $^{176}Yb/^{173}Yb$ = 0.79639 were used to calculate the instrumental mass bias of Hf and Yb isotope ratios, respectively.

4.2. Whole-Rock Geochemical Analysis

The Nuocang granodiorite samples selected for major and trace elemental analyses were conducted at the State Key Laboratory of Geological Processes and Mineral Resources, China University of Geosciences, Wuhan. The granodiorites were powdered into less than 200 mesh by a tungsten carbide ball mill, and finally, weighing ~0.5 g was selected for pulping. Major elements were analyzed by XRF, with an analytical uncertainty of <5%. Trace elements were measured with an Agilent 7500a ICP-MS. The analytical precision is better than 5% for elements with concentrations >10 ppm and less than 10% for those <10 ppm. The detailed analytical procedures are stated in [37].

4.3. Sr-Nd Isotopes

Sr-Nd isotopic measurements were conducted on the isotope dilution thermal ionization MS (TIMS) with a Triton Ti TIMS in the Zhongnan Mineral Resources Supervision and Test Center for Geoanalysis, Wuhan Center, China Geological Survey. The mixture of HF, HNO_3, and $HClO_4$ in Teflon bombs was used to dissolve the samples for Sr and Nd isotopic analyses. $^{86}Sr/^{88}Sr$ of 0.1194 and $^{146}Nd/^{144}Nd$ of 0.7219 were generally taken as the mass fractionation corrections [40].

5. Results

5.1. Zircon U-Pb Ages and Lu-Hf Isotopes

The length of zircon grains of Nuocnag granodiorites varies from 40 μm to 120 μm, with the 4:1 to 1:1 length-to-width ratios. The majority of the zircon grains in this study show clear oscillatory zoning, with no inherited core and metamorphic rim. Uranium contents of 542−1952 ppm, Th contents of 243−1369 ppm, with Th/U ratios of 0.37−0.70, suggesting a magmatic origin [41]. Zircons of NCNYT3 (18 spots) and NCNYT5 (20 spots) samples have $^{206}Pb/^{238}U$ ages ranging from 150.8 to 162.8 Ma and from 140.9 to 152.4 Ma, with weighted mean ages of 154.3 ± 1.3 Ma (2σ), and 150.9 ± 1.3 Ma (2σ), respectively (Figure 4, Table 1).

Table 1. Zircon LA-ICP-MS U-Pb dating result of Nuocang granodiorite.

Sample No.	Spot No.	Th	U	Th/U	$^{207}Pb/^{206}Pb$		$^{207}Pb/^{235}U$		$^{206}Pb/^{238}U$		$^{208}Pb/^{232}Th$		$^{207}Pb/^{235}U$		$^{206}Pb/^{238}U$	
		ppm	ppm		Ratio	1σ	Ratio	1σ	Ratio	1σ	Ratio	1σ	Age (Ma)	1σ	Age (Ma)	1σ
NCN-YT3	NCN-YT3-01	258.60	656.15	0.39	0.0495	0.0021	0.1605	0.0067	0.0237	0.0004	0.0495	0.0021	151.1	5.878640586	150.8	2.234167613
	NCN-YT3-02	243.45	651.98	0.37	0.0496	0.0019	0.1630	0.0061	0.0240	0.0003	0.0496	0.0019	153.4	5.310753674	152.7	2.187709109
	NCN-YT3-03	306.15	733.49	0.42	0.0493	0.0020	0.1630	0.0064	0.0241	0.0003	0.0493	0.0020	153.3	5.592835286	153.7	2.020804024
	NCN-YT3-04	1368.64	1951.75	0.70	0.0497	0.0014	0.1650	0.0044	0.0242	0.0003	0.0497	0.0014	155.0	3.804911278	154.0	1.802496621
	NCN-YT3-05	488.89	1042.87	0.47	0.0503	0.0018	0.1652	0.0059	0.0238	0.0003	0.0503	0.0018	155.2	5.169909843	151.9	1.755247831
	NCN-YT3-06	381.17	885.83	0.43	0.0510	0.0020	0.1697	0.0065	0.0244	0.0004	0.0510	0.0020	159.1	5.641800081	155.4	2.206600206
	NCN-YT3-07	370.03	787.74	0.47	0.0495	0.0021	0.1607	0.0064	0.0238	0.0003	0.0495	0.0021	151.3	5.622669297	151.5	2.064477891
	NCN-YT3-08	443.84	1007.72	0.44	0.0496	0.0022	0.1647	0.0071	0.0245	0.0004	0.0496	0.0022	154.8	6.161094504	156.0	2.208237054
	NCN-YT3-09	259.36	542.46	0.48	0.0506	0.0026	0.1648	0.0075	0.0241	0.0004	0.0506	0.0026	154.9	6.543424564	153.4	2.331191049
	NCN-YT3-11	368.28	787.98	0.47	0.0501	0.0024	0.1668	0.0074	0.0244	0.0003	0.0501	0.0024	156.7	6.442724526	155.4	2.201532889
	NCN-YT3-13	895.79	1526.41	0.59	0.0480	0.0016	0.1607	0.0056	0.0242	0.0003	0.0480	0.0016	151.4	4.914979083	154.3	1.916805401
	NCN-YT3-14	254.43	583.03	0.44	0.0512	0.0020	0.1699	0.0068	0.0241	0.0003	0.0512	0.0020	159.3	5.899657767	153.7	2.078019071
	NCN-YT3-15	1080.34	1639.74	0.66	0.0497	0.0014	0.1668	0.0047	0.0243	0.0003	0.0497	0.0014	156.7	4.120652056	155.0	1.742173735
	NCN-YT3-16	458.25	844.57	0.54	0.0499	0.0022	0.1631	0.0066	0.0238	0.0003	0.0499	0.0022	153.4	5.751187756	151.5	2.031091286
	NCN-YT3-18	426.78	972.84	0.44	0.0500	0.0020	0.1659	0.0060	0.0242	0.0003	0.0500	0.0020	155.9	5.253441493	154.4	1.844105038
	NCN-YT3-19	815.99	1246.69	0.65	0.0506	0.0017	0.1694	0.0059	0.0242	0.0003	0.0506	0.0017	158.9	5.086706758	154.2	1.871192917
	NCN-YT3-21	869.70	1444.21	0.60	0.0501	0.0020	0.1760	0.0068	0.0256	0.0003	0.0501	0.0020	164.6	5.856328883	162.8	2.090853914
	NCN-YT3-23	335.23	748.48	0.45	0.0500	0.0025	0.1674	0.0080	0.0247	0.0003	0.0500	0.0025	157.1	6.935594206	157.2	2.037402207

Table 1. *Cont.*

Sample No.	Spot No.	Th	U	Th/U	$^{207}Pb/^{206}Pb$		$^{207}Pb/^{235}U$		$^{206}Pb/^{238}U$		$^{208}Pb/^{232}Th$		$^{207}Pb/^{235}U$		$^{206}Pb/^{238}U$	
		ppm	ppm		Ratio	1σ	Ratio	1σ	Ratio	1σ	Ratio	1σ	Age (Ma)	1σ	Age (Ma)	1σ
NCN-YT5	NCN-YT5-01	279.33	690.59	0.40	0.05017	0.00322	0.15657	0.00901	0.02320	0.00035	0.05017	0.00322	147.7	7.915054148	147.9	2.206005581
	NCN-YT5-03	403.97	817.81	0.49	0.05226	0.00226	0.17136	0.00712	0.02411	0.00031	0.05226	0.00226	160.6	6.175466477	153.6	1.962492186
	NCN-YT5-04	312.18	692.27	0.45	0.04934	0.00217	0.16768	0.00712	0.02490	0.00035	0.04934	0.00217	157.4	6.1947696	158.6	2.209765425
	NCN-YT5-05	348.26	840.72	0.41	0.04959	0.00236	0.15693	0.00693	0.02344	0.00032	0.04959	0.00236	148.0	6.083826678	149.4	2.001305011
	NCN-YT5-06	456.80	1013.02	0.45	0.04936	0.00207	0.16067	0.00637	0.02396	0.00034	0.04936	0.00207	151.3	5.571610871	152.7	2.126633394
	NCN-YT5-07	295.09	748.58	0.39	0.04990	0.00230	0.16008	0.00741	0.02344	0.00035	0.04990	0.00230	150.8	6.488635488	149.3	2.204384254
	NCN-YT5-08	416.44	907.85	0.46	0.05084	0.00290	0.16130	0.00770	0.02369	0.00034	0.05084	0.00290	151.8	6.736998527	150.9	2.166674393
	NCN-YT5-09	575.48	1050.06	0.55	0.04930	0.00202	0.15457	0.00634	0.02280	0.00029	0.04930	0.00202	145.9	5.579278375	145.3	1.825797051
	NCN-YT5-10	261.94	662.29	0.40	0.05248	0.00235	0.17372	0.00727	0.02436	0.00037	0.05248	0.00235	162.6	6.293287554	155.2	2.342009655
	NCN-YT5-11	346.37	769.47	0.45	0.04923	0.00226	0.15681	0.00696	0.02339	0.00033	0.04923	0.00226	147.9	6.109559884	149.0	2.055673905
	NCN-YT5-12	346.64	895.59	0.39	0.04921	0.00188	0.16228	0.00608	0.02390	0.00034	0.04921	0.00188	152.7	5.310899944	152.2	2.119258927
	NCN-YT5-13	307.73	820.19	0.38	0.04952	0.00205	0.15668	0.00622	0.02312	0.00030	0.04952	0.00205	147.8	5.464077401	147.4	1.887466747
	NCN-YT5-14	340.90	761.79	0.45	0.05228	0.00227	0.17067	0.00726	0.02386	0.00032	0.05228	0.00227	160.0	6.296839221	152.0	2.019284285
	NCN-YT5-17	328.08	682.89	0.48	0.04944	0.00222	0.15800	0.00683	0.02345	0.00032	0.04944	0.00222	149.0	5.987072839	149.4	2.004429465
	NCN-YT5-18	278.66	659.22	0.42	0.04997	0.00233	0.15949	0.00726	0.02352	0.00033	0.04997	0.00233	150.3	6.357828411	149.9	2.107184755
	NCN-YT5-19	293.62	644.80	0.46	0.05059	0.00242	0.16203	0.00730	0.02376	0.00031	0.05059	0.00242	152.5	6.379606547	151.4	1.941662278
	NCN-YT5-20	476.04	859.00	0.55	0.04982	0.00211	0.16132	0.00662	0.02384	0.00031	0.04982	0.00211	151.9	5.79314197	151.9	1.925953949
	NCN-YT5-22	531.88	1060.19	0.50	0.04970	0.00188	0.16278	0.00601	0.02399	0.00029	0.04970	0.00188	153.1	5.245983248	152.8	1.81947249
	NCN-YT5-24	444.32	849.10	0.52	0.04973	0.00202	0.15861	0.00612	0.02346	0.00029	0.04973	0.00202	149.5	5.366659227	149.5	1.837156843
	NCN-YT5-25	458.12	1046.00	0.44	0.04928	0.00171	0.16215	0.00560	0.02392	0.00028	0.04928	0.00171	152.6	4.892766152	152.4	1.793306592

Ten Lu-Hf isotopic analyses were conducted on the NCNYT3 sample, with the $^{176}Lu/^{177}Hf$ ratios of 0.001113–0.002631 and $^{176}Hf/^{177}Hf$ ratios of 0.282109–0.282560, yielding εHf(t) values from −10.8 to −5.0 (Table 2).

Table 2. Hf isotope analysis result of Nuocang granodiorite.

Spot No.	^{176}Hf/^{177}Hf	1σ	^{176}Lu/^{177}Hf	1σ	^{176}Yb/^{177}Hf	1σ	age	εHf(t)	T^2_{DM} (Ma)
NCN-YT5-05	0.282405	0.000023	0.001591	0.000006	0.060679	0.004838	149	−9.86	1823
NCN-YT5-06	0.282429	0.000021	0.001375	0.000007	0.025070	0.000139	153	−8.93	1768
NCN-YT5-08	0.282425	0.000029	0.001222	0.000014	0.027063	0.000261	151	−9.07	1775
NCN-YT5-09	0.282427	0.000027	0.001708	0.000021	0.054536	0.000378	145	−9.18	1778
NCN-YT5-11	0.282377	0.000025	0.001399	0.000007	0.018755	0.000416	149	−10.84	1885
NCN-YT5-12	0.282421	0.000029	0.001428	0.000017	0.084494	0.002635	152	−9.21	1785
NCN-YT5-13	0.282385	0.000030	0.001571	0.000006	0.029334	0.000315	147	−10.63	1870
NCN-YT5-14	0.282439	0.000028	0.001016	0.000004	0.037709	0.000561	152	−8.54	1743
NCN-YT5-19	0.282439	0.000036	0.001348	0.000006	0.023860	0.000727	151	−8.60	1746
NCN-YT5-22	0.282460	0.000038	0.001383	0.000015	0.028526	0.000683	153	−7.83	1699
NCN-YT5-24	0.282541	0.000038	0.001368	0.000020	0.031809	0.000406	150	−5.04	1520

5.2. Major and Trace Elements

Major and trace element data of Nuocang granodiorites are listed in Table 3. They have narrow ranges of SiO_2 (64.37–65.02 wt%), low K_2O (1.58–2.09 wt%) and Na_2O (2.13–2.26 wt%), moderate MgO (1.73–1.77 wt%), and high Al_2O_3 (16.15–16.39 wt%), indicating the medium K calc-alkaline and peraluminous characteristics (Figure 5a–c). The rare earth elements composition in this study is less variable, with REEs of 97.0–111.0, LREE/HREE of 6.12–7.19, $(La/Yb)_N$ of 6.5–8.3, and δEu values of 0.77–0.81 (average = 0.79). The REE pattern revealed the enrichment in LREEs and depletion in HREEs (Figure 6a; [41]). The Nuocang granodiorite samples are enriched in the Rb, K, Zr, Hf, U, and Th but depleted in Sr, Ba, Nb, Ti, and P (Figure 6b). Sr/Y ratios of 9.7–11.4, with Y contents of 16.0– 20.9 ppm, indicate typical arc magmatic rocks [42].

Table 3. Major and trace element analysis result of Nuocang granodiorite (major elements: wt%; trace elements: ppm).

Sample No.	NCN-YT1	NCN-YT2	NCN-YT3	NCN-YT4	NCN-YT5	NCN-YT6
SiO_2	65.02	64.94	64.48	64.37	64.87	64.68
Al_2O_3	16.23	16.13	16.21	16.39	16.22	16.15
Fe_2O_3	0.93	0.92	1.02	0.77	0.94	0.78
FeO	4.17	4.15	4.12	4.33	4.23	4.27
CaO	4.95	4.91	4.91	5.39	4.48	4.90
MgO	1.75	1.73	1.76	1.77	1.77	1.74
K_2O	1.58	1.91	2.09	1.77	1.99	2.07
Na_2O	2.14	2.12	2.21	2.17	2.26	2.13
TiO_2	0.56	0.55	0.58	0.58	0.58	0.55
P_2O_5	0.10	0.10	0.09	0.10	0.09	0.09
MnO	0.09	0.09	0.09	0.09	0.09	0.08

Table 3. *Cont.*

Sample No.	NCN-YT1	NCN-YT2	NCN-YT3	NCN-YT4	NCN-YT5	NCN-YT6
LOI	1.81	1.79	1.78	1.59	1.81	1.88
Total	99.34	99.34	99.34	99.32	99.33	99.33
TFe_2O_3	5.57	5.53	5.59	5.58	5.64	5.53
Mg#	0.38	0.38	0.38	0.39	0.38	0.38
A/CNK	1.14	1.11	1.09	1.07	1.16	1.10
A/NK	3.10	2.90	2.75	2.99	2.76	2.81
Rb	54.98	74.27	78.66	63.06	74.14	76.69
Ba	275.48	292.48	316.57	289.71	282.99	297.35
Th	9.51	11.07	9.12	8.89	9.04	9.15
U	1.26	1.23	1.19	0.95	1.17	1.20
Nb	7.23	8.14	7.12	7.19	7.34	6.72
Sr	202.11	203.01	222.51	196.14	220.56	212.21
Zr	129.56	125.34	127.99	133.67	131.42	127.50
Hf	3.23	3.23	3.06	3.57	3.57	3.40
La	23.36	22.60	19.45	21.42	20.17	23.44
Ce	43.57	42.84	37.46	40.90	39.57	44.18
Pr	5.58	5.32	4.84	5.19	4.87	5.66
Nd	19.37	18.48	17.19	18.14	17.34	19.51
Sm	3.86	3.53	3.53	3.62	3.60	3.72
Eu	1.01	0.93	0.94	0.98	0.92	0.94
Gd	3.75	3.71	3.63	3.79	3.62	3.77
Tb	0.62	0.61	0.61	0.61	0.60	0.62
Dy	3.73	3.66	3.69	3.68	3.62	3.70
Ho	0.78	0.75	0.75	0.74	0.73	0.73
Er	2.20	2.14	2.16	2.06	2.03	2.09
Tm	0.34	0.33	0.33	0.32	0.33	0.32
Yb	2.16	2.18	2.14	2.07	2.09	2.02
Lu	0.34	0.33	0.33	0.31	0.32	0.30
Y	20.92	19.49	19.79	19.80	19.40	19.66
ΣREE	110.66	107.41	97.03	103.83	99.81	111.01
LREE	96.75	93.70	83.40	90.24	86.47	97.45
HREE	13.91	13.71	13.63	13.58	13.34	13.55
LREE/HREE	6.95	6.83	6.12	6.64	6.48	7.19
La_N/Yb_N	7.77	7.43	6.52	7.42	6.93	8.32
δEu	0.81	0.79	0.81	0.81	0.78	0.77
δCe	0.94	0.96	0.95	0.95	0.98	0.94
Zr-saturation T (°C)$_{avrg}$	719	711	709	709	722	711
Ap-saturation T (°C)	804	803	797	795	802	799

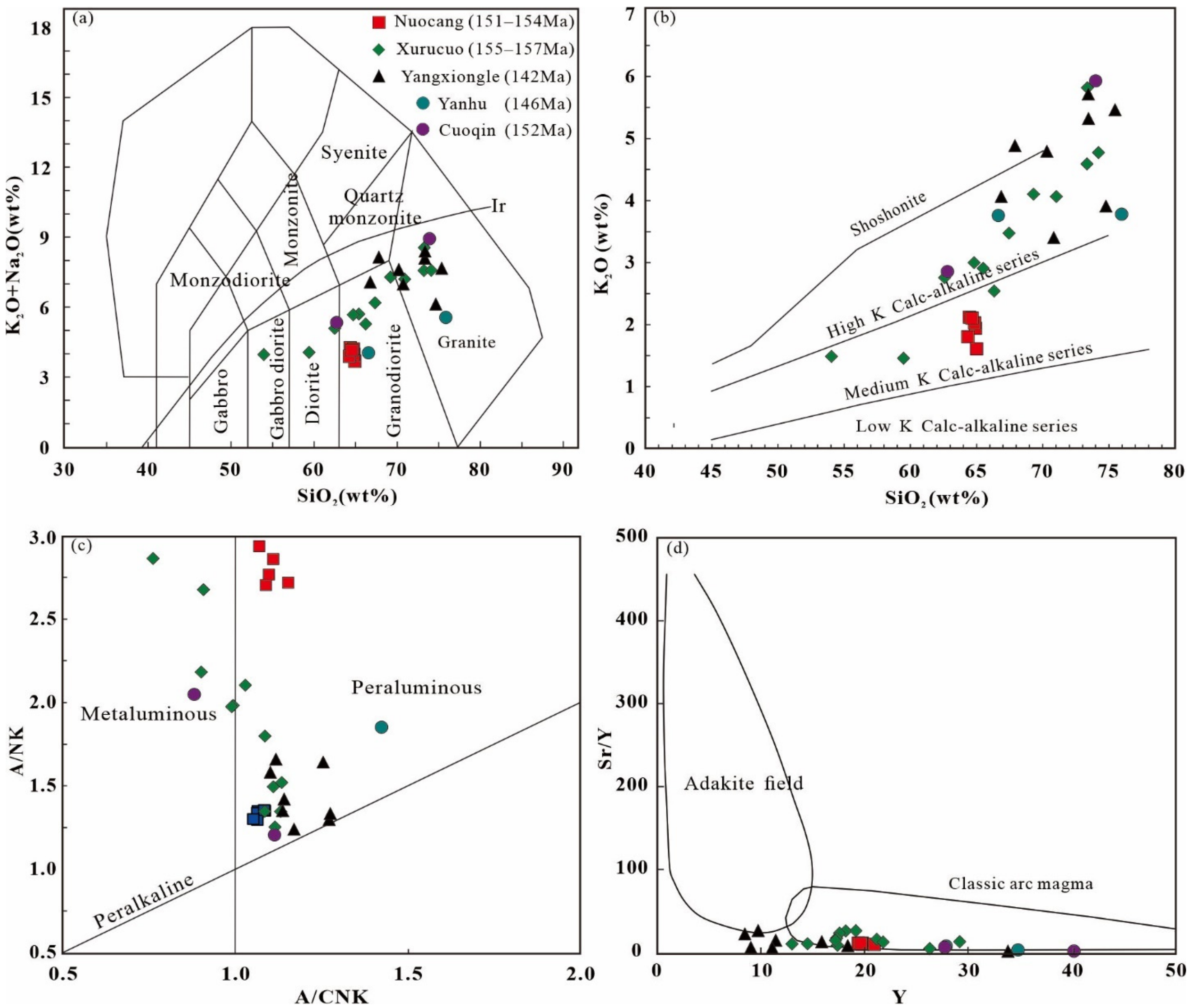

Figure 5. (**a**) $K_2O + Na_2O$ vs. SiO_2 diagram [43]; (**b**) K_2O vs. SiO_2 diagram [44]; (**c**) A/NK vs. A/CNK diagram [45]; (**d**) Sr/Y vs. Y diagram [45]. Data sources: Nuocang granodiorites from this study; Xurucuo granitoids [16]; Yangxiongle granitoids [23]; Yanhu and Cuoqin granitoids [4].

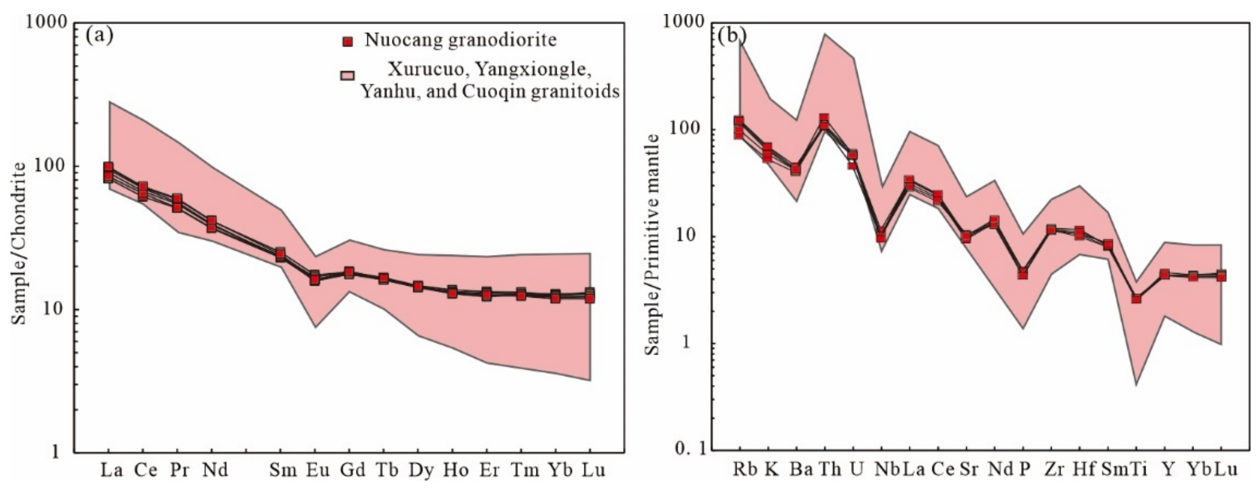

Figure 6. Chondrite normalized REE distribution diagram (**a**) and primitive mantle normalized trace element spider diagram (**b**) [46] for Nuocang granodiorites. Data are from the same source as Figure 5.

5.3. Sr-Nd Isotopes

Sr-Nd isotopic results of Nuocang granodiorites are shown in Table 4. They have nonradiogenic or negative isotope compositions, with the $^{87}Sr/^{86}Sr$ ratios ranging from 0.714343 to 0.714578 and $^{143}Nd/^{144}Nd$ ratios ranging from 0.512066 to 0.512098, corresponding to $(^{87}Sr/^{86}Sr)i$ ratios of 0.712231–0.712619 and εNd(t) values from −9.56 to −8.99. Their two-stage Nd model ages ($T^2{}_{DM}$) range from 1.45 to 1.49 Ga.

Table 4. Sr–Nd isotopic data for the Nuocang granodiorites.

Sample No.	Age (Ma)	$^{87}Rb/^{86}Sr$	$^{87}Sr/^{86}Sr$	±2σ	$(^{87}Sr/^{86}Sr)_i$	$^{147}Sm/^{144}Nd$	$^{143}Nd/^{144}Nd$	±2σ	$(^{143}Nd/^{144}Nd)_i$	$\varepsilon_{Nd(t)}$	$T_2{}^{DM}$(Ma)
NCN-YT1	154	0.787580	0.714343	0.000006	0.712619	0.12030	0.512084	0.000002	0.51196278	−19.31	1468
NCN-YT2	154	1.059180	0.714550	0.000008	0.712231	0.11544	0.512066	0.000009	0.511949671	−9.56	1486
NCN-YT3	154	1.023500	0.714524	0.000008	0.712283	0.12399	0.512098	0.000005	0.511973061	−9.11	1454
NCN-YT4	151	0.930830	0.714518	0.000012	0.712480	0.12047	0.512097	0.000003	0.511975611	−9.06	1451
NCN-YT5	151	0.973190	0.714483	0.000009	0.712353	0.12554	0.512098	0.000007	0.5119715	−9.14	1456
NCN-YT6	151	1.046290	0.714578	0.000007	0.712287	0.11523	0.512095	0.000005	0.511978886	−8.99	1446

Note: $\varepsilon_{Nd\,(t)} = [(^{143}Nd/^{144}Nd)_{sample(t)}/(^{143}Nd/^{144}Nd)_{CHUR(t)} - 1] \times 10^{-4}$; $T_{DM2} = 1/\lambda \times \{1 + [(^{143}Nd/^{144}Nd)_{sample} - ((^{147}Sm/^{144}Nd)_{sample} - (^{147}Sm/^{144}Nd)_{crust}) \times (e^{\lambda t} - 1) - (^{143}Nd/^{144}Nd)_{DM}]/((^{147}Sm/^{144}Nd)_{crust} - (^{147}Sm/^{144}Nd)^{DM})\}$. $(^{147}Sm/^{144}Nd)_{CHUR} = 0.1967$, $(^{143}Nd/^{144}Nd)_{CHUR} = 0.512638$, $(^{147}Sm/^{144}Nd)_{DM} = 0.2137$, $(^{143}Nd/^{144}Nd)_{DM} = 0.51315$, $(^{147}Sm/^{144}Nd)_{crust} = 0.1012$.

6. Discussion

6.1. The Mid-Late Jurassic Magmatism in the Gangdese of Southern Lhasa Terrane

The previous research on the magmatic rocks of Lhasa terrane suggests that the Mid-Late Jurassic magmatism dominantly occurred in the central (e.g., Yangxiongle intrusion, 142.0 Ma, [23]; Wenbu intrusion, 154.5 Ma, Xie Guogang et al., unpublished data; Xiadingle intrusion, 153.1 Ma, Liu Dengzhong et al., unpublished data; Xiongba intrusion, 149.0 Ma; and Jiangba intrusion, 170 Ma; [7]; Cuoqin granite, 152.0 Ma; and Yanhu rhyolite, 146.0 Ma, [4]; Xurucuo, 155.1 and 155.7 Ma, [16]) and northern part of Lhasa terrane (e.g., Nierong intrusion, 175 Ma, [47]; Darucuo andesite, 165.0 Ma, [15]). However, the Gangdese Batholith and volcanic rocks in the Gangdese of the southern Lhasa terrane predominantly consist of Paleocene-Eocene, Miocene, and Cretaceous magmatic rocks [9,27]. Recent work has identified the presence of the Mid-Late Jurassic magmatic rocks in the eastern Gangdese of southern Lhasa terrane, such as the Xietongmen (177 Ma, [26]), Tangbai (180 Ma, [11]), Wobu (166 Ma, [26]), Dazhuqu (174 Ma, [5]), and Nymo intrusions (178 Ma, [9,27]). In addition, the intrusions that occurred in the Zedong area were formed in the Late Jurassic (160–155 Ma; [26]), which possibly represent a slice of magmatic arc developed on the southern margin of the Lhasa Terrane [26]; Figure 1c). Correspondingly, the volcanic rocks of the Sangri Formation formed in the same period widely developed in the southern Lhasa terrane, with a wide age range of 195–137 Ma [12]. In this study, we identified the Late Jurassic intrusion in the Nuocang district for the first time, which expands the distribution of the Mid-Late Jurassic magmatism in the southern Lhasa terrane.

6.2. Petrogenesis of Nuocang Granitoid Rocks

Traditionally, four types of granite (I, S, M, and A) have been divided based on mineralogical and geochemical characteristics [48]. A-type granitoids were first excluded since the Nuocang granodiorites lack anhydrous minerals and depletion of high field-strength elements (Figure 6b), with relatively low magmatic crystallization temperatures of 697–804°C (the Zr-saturation temperature of 697–733 °C [49], and the Ap-saturation temperature ranging from 795 to 804 °C [50]; A-type granite is usually higher than 850 °C [51]). The Nuocang granodiorites, together with other Jurassic granitoids in the Lhasa terrane, show features of calc-alkaline to high-K calc-alkaline. The granodiorites have high Al_2O_3 (16.13–16.39), with the A/CNK values of 1.07– 1.16, showing similarities with S-type granite [52]. However, the positive correlation between Rb and Th and negative correlation between Rb and Y

(Figure 7a,b) are similar to these I-type granitoids in the central Lhasa terrane [7,16,52]. Moreover, The Nuocang granodiorites and other Jurassic granite in the Lhasa terrane totally fall in the I-type granite scope, indicating that they should be I-type granite rather than S-type (Figure 7c,d).

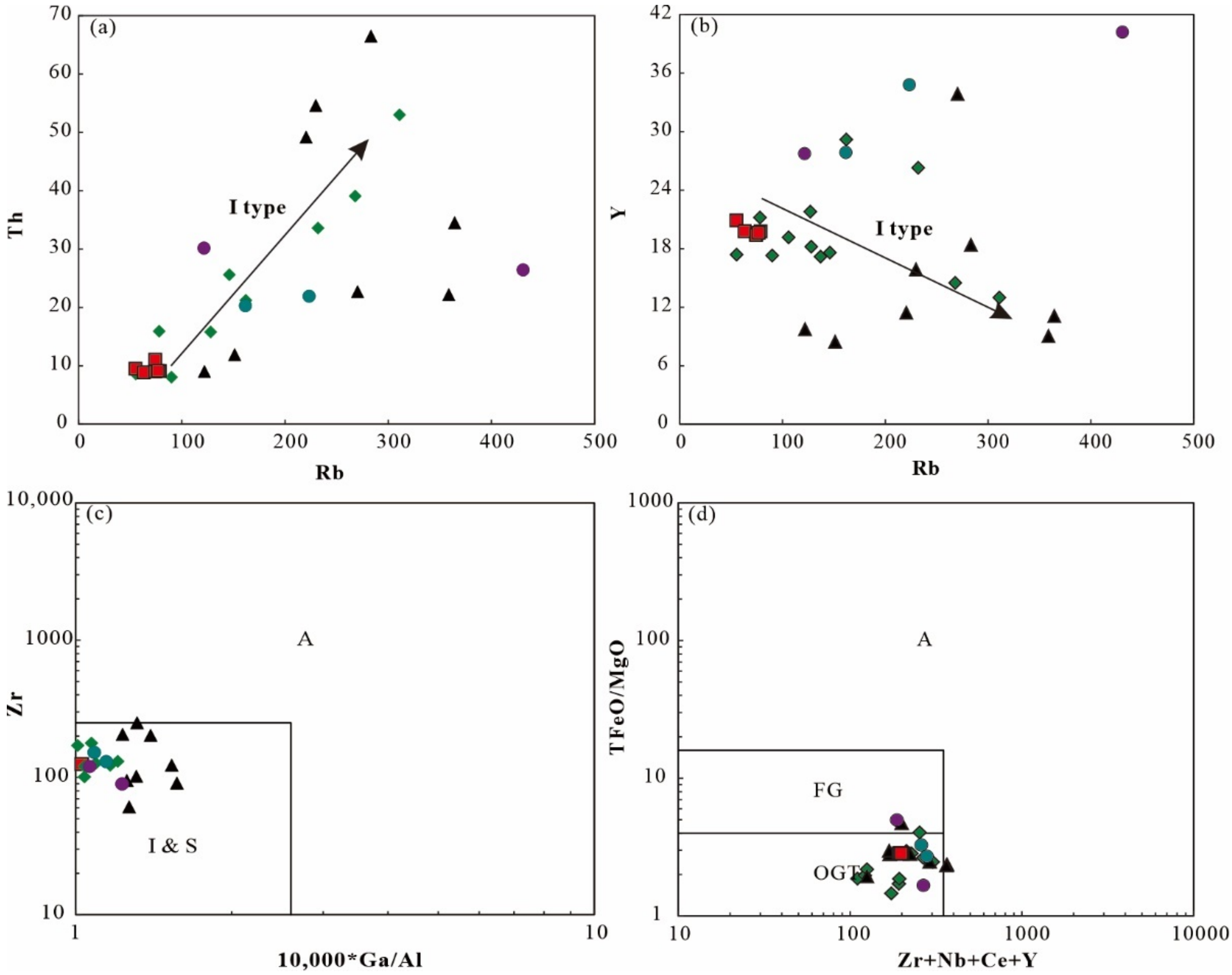

Figure 7. (**a**) P_2O_5 vs. SiO_2 diagram; (**b**) Th vs. Rb diagram; (**c**) Y vs. Rb diagram; (**d**) TFeO/MgO vs. Zr+Nb+Ce+Y diagram [53].

Three formation mechanisms for the I-type granite have been proposed: (1) extensive fractional crystallization of mantle-derived magmas, probably accompanied by crustal assimilation [54,55], (2) partial melting of crustal materials [56], and (3) magma mixing mechanism of the mantle- and crust-derived magmas [57,58]. Magmas generated by fractional crystallization of mantle-derived parental magmas generally show relatively high εNd(t) and εHf(t) values and develop the mafic to felsic magmatic rocks in the surroundings [54,55]. The Nuocang granodiorites show lower εNd(t) values (from −9.56 to −8.99) and εHf(t) values (from −10.8 to −5.0), with no mafic intrusions in the surrounding area. Moreover, the variation of La/Nd values versus SiO_2 (Figure 8a) and linear relation on the La/Sm versus La plot (Figure 8b) correspond to the partial melting process.

The lower Sm/Yb (mean 1.73) and La/Sm ratios (mean 5.97) of Nuocang granodiorites were plotted into the range of pyroxene-dominated residual mineralogy in the discrimination diagram (Figure 8c), suggesting a relatively low-pressure condition and shallow magma source [59]. Hence, the partial melting of crustal materials possibly contributed to the magma source of Nuocang granodiorites.

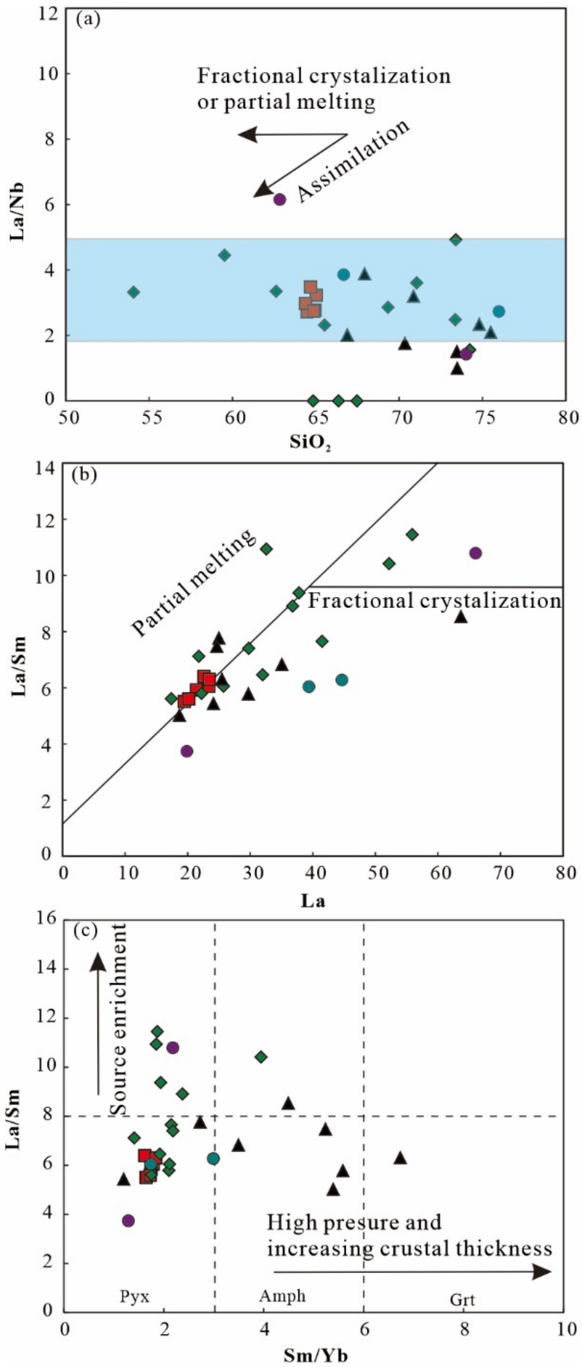

Figure 8. (**a**) La/Nb vs. SiO_2 diagram; (**b**) La/Sm vs. La diagram; (**c**) La/Sm vs. Sm/Yb diagram [60]. Data are from the same source as Figure 5.

Isotopically, the Nuocang granodiorites show negative Hf isotope values (from −10.8 to −5.0), and old $T_{DM}{}^{c}$ values (from 1.52 to 1.88 Ga) of the igneous rocks, plot into the area of Middle Jurassic granitoids summarized by researchers, suggesting the Archean-Proterozoic Nyainqentanglha basement rocks of ancient Lhasa crust may exist in the Nuocang district (Figure 9a). This viewpoint also has been identified by the Late Cretaceous granite porphyry nearby (Hf isotope values: from −22.0 to −6.0; [21]). Similarly, the Nuocang granodiorites display remarkably high $(^{87}Sr/^{86}Sr)_i$ (from 0.712231 to 0.712619), low εNd(t) (from −9.56 to −8.99) values, and old T_{DM2}(Nd) ages (from 1.45 to 1.49 Ga; Figure 9b), strongly suggest that the ancient Lhasa crust exists in the Nuocang district. This supports the interpretation suggesting that there exists an ancient Lhasa crust in western Gangdese (83–87° E) and southern Lhasa terrane by [20].

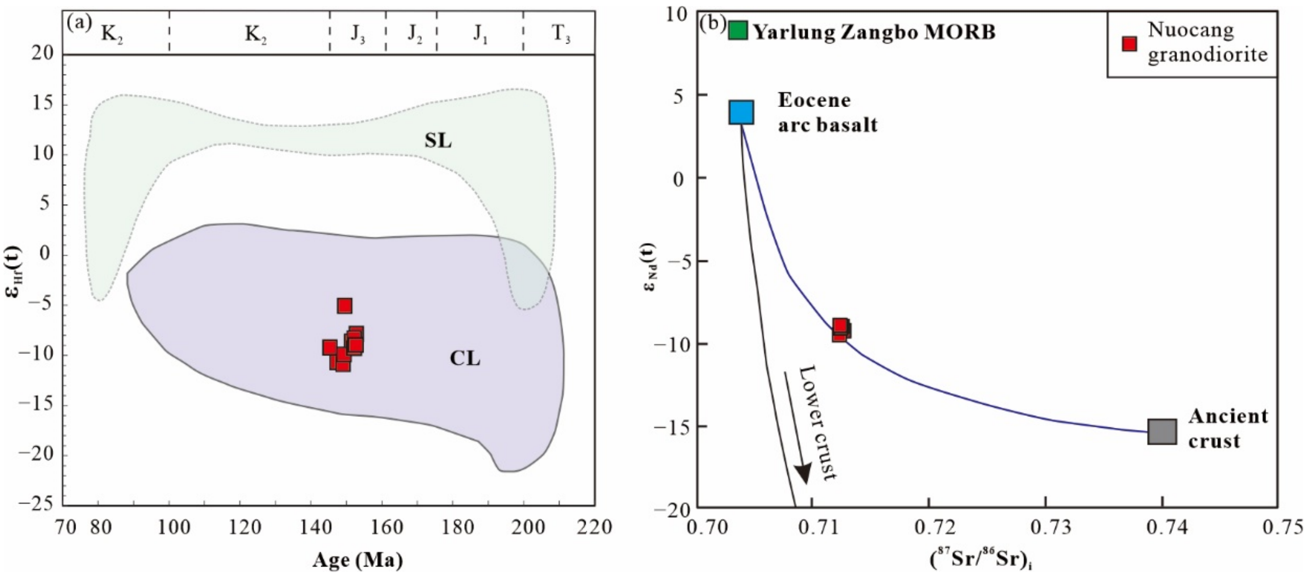

Figure 9. (**a**) εHf(t) vs. U-Pb age diagram of zircons from the Nuocang granodiorites; (**b**) $^{87}Sr/^{86}Sr(i)$ vs. εNd(t) for the Nuocang granodiorites. CL- the Hf values of granitoids in the central Lhasa terrane; SL- the Hf values of granitoids in the southern Lhasa terrane; The Yarlung Zangbo Mid-ocean ridge basalts (MORB) is from [4]: εNd(t) = +7.0, Nd = 1.2 ppm; The mantle-derived basaltic magmas (represented by the Dazi basalt; [59]): $(^{87}Sr/^{86}Sr)i$ = 0.7043, εNd(t) = +5.2, Sr = 291 ppm, Nd = 9.6 ppm; Ancient crustal (represented by a strongly peraluminous granites from the central Lhasa terrane; [4]): (87Sr/86Sr)i = 0.7402, εNd(t) = −15.4, Sr = 131 ppm, Nd = 43.40 ppm. The central Lhasa terrane is from [4,20].

Notably, the εHf(t) values of Nuocang granodiorites show a heterogeneous feature (vary from −10.8 to −5.0), indicating a magma mixing with mantle-derived sourced compositions [51]. The Sr-Nd isotopic data plotted along the mixing lines of the mantle-derived and the ancient Lhasa crustal materials (Figure 9b) in the $^{87}Sr/^{86}Sr(i)$ vs. εNd(t) diagram, together with the Mg# (38–39), lower $(La/Yb)_N$ (6.52–8.32) and $(Gd/Yb)_N$ (1.40–1.54) ratios, also revealing the involving input of mantle melt. Consequently, we proposed that the Nuocang granodiorites originated from the partial melting of ancient Lhasa crust, with the contribution of mantle-derived melt.

6.3. Implication for the Jurassic Neo-Tethys Geodynamic Model in the Gangdese of Southern Lhasa Terrane

As widely accepted that the Neo-Tethys Oceanic opening started from Carboniferous-Early Permian time [61,62], and the Lhasa terrane separated from Gondwanaland before Triassic [63]. Subsequently, the crustal accretion and tectonic-magmatic evolution of Lhasa terrane from Triassic to Cretaceous was triggered by the southward subduction of Bangong-Nujiang oceanic crust and northward subduction of Neo-Tethys oceanic crust [64,65]. However, the Mesozoic tectonic-magmatic evolutional model in the Gangdese of southern Lhasa terrane has always been debated. These competing models include (1) the southward subduction of the Bangong-Nujiang oceanic crust that formed in a back-arc extensional setting [4,16,64,66] and (2) the northward subduction of Neo-Tethys oceanic crust [1,5,10,12,14] that represents an Andean-type continental margin. Previous researchers proposed that the initial Neo-Tethys subduction began in the early Cretaceous based on that the dating of remnant ophiolites in the Yarlung Zangbo suture was Late Jurassic [67]. Thus, some scholars proposed that the Gangdese magmatism formed in a back-arc environment during the Mid-Late Triassic-Jurassic [64].

However, extensive Mid-Late Triassic–Jurassic magmas, such as the volcanic rocks of Yeba Formation and Sangri Group and the coeval intrusions, have been identified in the Gangdese of southern Lhasa terrane, which formed a continuous E–W-trending liner magmatic belt adjacent to the Yarlung Zangbo suture zone [1,11,12,17,66]. These Mid-Late Triassic-Jurassic magmatic rocks are featured by the subducted magmas that formed in a continental arc setting, showing the affinity with the northward subduction of the Neo-Tethys ocean [10,14,17]. The Nuocang granodiorites show enrichment in LREE and LILEs, and depletion in HREE and HFSEs, which are typical of arc-related magmatic rocks [68]. Additionally, on the trace element discrimination diagram, all the samples plot within the arc field (Figure 10a,b) [69]. The Th/Ta ratios of Nuocang granodiorites are greater than 6 (mean value = 10.75), which suggests an active continental margin setting (Figure 10c).

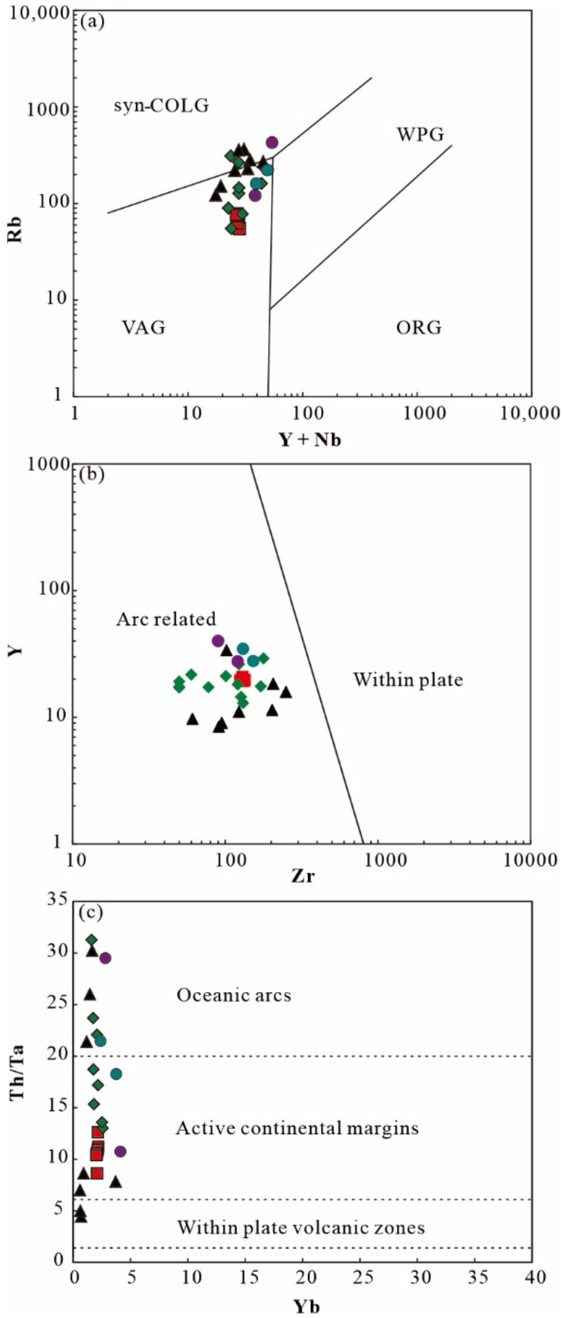

Figure 10. (**a**) Rb vs. Y + Nb [69]; (**b**) Y vs. Zr; (**c**) Th/Ta vs. Y [70]. Data are from the same source as Figure 5.

Therefore, we proposed that Nuocang granodiorites formed in an active continental margin setting associated with the subduction of Neo-Tethys oceanic crust during the Late Jurassic. During the Late Jurassic, the northward subduction of Neo-Tethys oceanic crust induced the partial melting of a depleted mantle wedge that had been metasomatized by subduction-related fluids and generated the initial basaltic magmas. With the upwelling of basalt magmas, it underplated and produced significant thermal perturbation to cause the partial melting of the overlying ancient Lhasa crust in the Nuocang district. Partial melting of ancient Lhasa crust, mixing with the mantle materials, was responsible for the Nuocang granodiorites (Figure 11a,b).

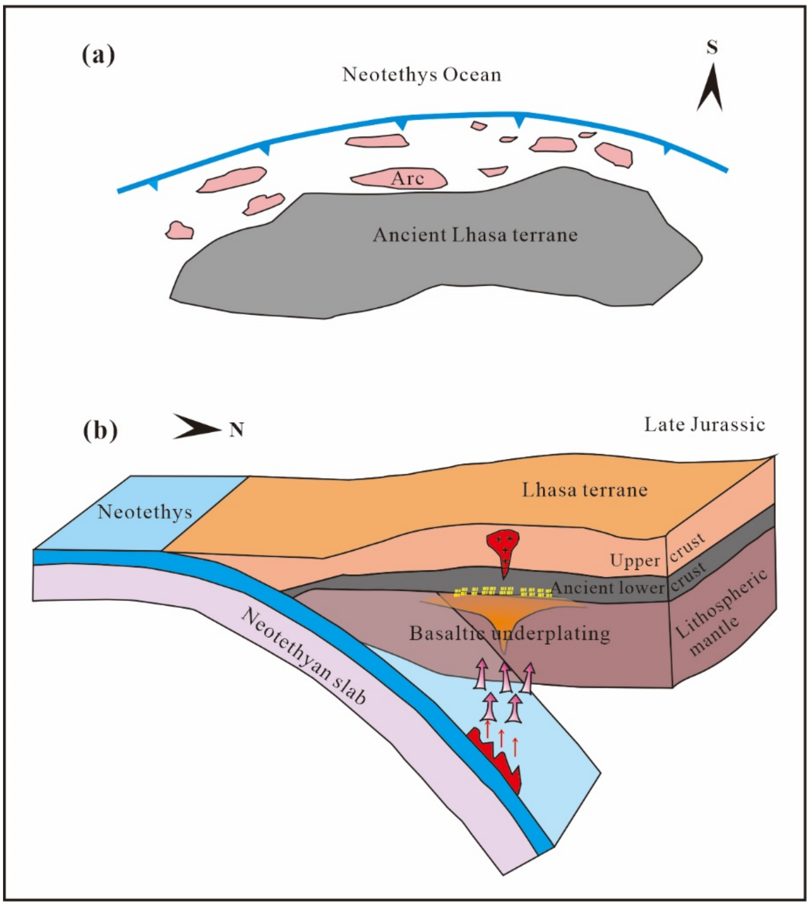

Figure 11. (**a**) Cartoon model of multiple terranes and island arcs in Late Jurassic, Lhasa Terrane; (**b**) cartoon showing dynamic model of the Neo–Tethys ocean subduction and formation of Nuocang granodiorites during the Late Jurassic, southern Lhasa terrane.

7. Conclusions

(1) Zircon U-Pb dating of two Nuocang granodiorites shows weighted mean ages of 151–154 Ma, firstly revealing that the Late Jurassic granitoids also occurred in the western Gangdese of southern Lhasa terrane.

(2) Major and trace elements and Sr-Nd-Hf isotopic data indicate that the Nuocang granodiorites were sourced from the partial melting of ancient Lhasa crust, with the contribution of mantle-derived materials involved during their generation.

(3) The Nuocang granodiorites possibly formed in an active continental margin setting. They record the late Jurassic magmatism in western Gangdese, which were the product of the northward subduction of the Neo-Tethys oceanic crust beneath the Lhasa terrane.

Author Contributions: J.J., B.B., and S.G. conceived this contribution and conducted all field and analytical work, assisted by P.H. (Peng Hu), X.C., K.T., P.H. (Pengcheng Hu), J.H., and X.G. The manuscript was written by J.J., B.B., and S.G., with contributions from P.H. (Peng Hu), X.C., K.T., P.H. (Pengcheng Hu), J.H., and X.G. All authors have read and agreed to the published version of the manuscript.

Funding: This research is supported by the Open Research Fund Program (2021YSJS09) of the Key Laboratory of Metallogenic Prediction of Nonferrous Metals and Geological Environment Monitoring (Central South University), Ministry of Education, the China Geological Survey (DD20221802, DD20201153, DD20190443, DD20190159-33, DD20160027-2), National Key Research and Development Program of China (No. 2016YFC0600300), and Commonwealth Project from the Ministry of Land and Resources (201511015).

Data Availability Statement: Not Applicable.

Acknowledgments: Staff at Wuhan Sample Solution Analytical Technology Co., Ltd., Zhongnan Mineral Resources Supervision and Test Center for Geoanalysis, Wuhan Center, China Geological Survey, and the State Key Laboratory of Geological Processes and Mineral Resources, China University of Geosciences, Wuhan are gratefully acknowledged for assistance with the instrument operation. We thank the reviewers for the journal Minerals.

Conflicts of Interest: The authors declare no conflict of interest.

References

1. Chu, M.F.; Chung, S.L.; Song, B.; Liu, D.Y.; O'Reilly, S.Y.; Pearson, N.J. Zircon U–Pb and Hf isotope constraints on the Mesozoic tectonics and crustal evolution of southern Tibet. *Geology* **2006**, *34*, 745–748. [CrossRef]
2. Guan, Q.; Zhu, D.C.; Zhao, Z.D.; Dong, G.C.; Mo, X.X.; Liu, Y.S.; Hu, Z.C.; Yuan, H.L. Zircon U–Pb chronology, geochemistry of the Late Cretaceous mafic magmatism in the southern Lhasa Terrane and its implications. *Acta Petrol. Sin.* **2011**, *27*, 2083–2094. (In Chinese with English Abstract)
3. Schärer, U.; Xu, R.H.; Allegre, C.J. U–Pb geochronology of Gangdese (Transhimalaya) plutonism in the Lhasa-Xigaze region, Tibet. *Earth Planet. Sci. Lett.* **1984**, *69*, 311–320. [CrossRef]
4. Zhu, D.C.; Zhao, Z.D.; Niu, Y.L.; Mo, X.X.; Chung, S.L.; Hou, Z.Q.; Wang, L.Q.; Wu, F.Y. The Lhasa Terrane: Record of a micro continent and its histories of drift and growth. *Earth Planet. Sci. Lett.* **2011**, *301*, 241–255. [CrossRef]
5. Ji, W.Q.; Wu, F.Y.; Chung, S.L.; Li, J.X.; Liu, C.Z. Zircon U–Pb geochronology and Hf isotopic constraints on petrogenesis of the Gangdese batholith, southern Tibet. *Chem. Geol.* **2009**, *262*, 229–245. [CrossRef]
6. Ji, W.Q.; Wu, F.Y.; Liu, C.Z.; Chung, S.L. Early Eocene crustal thickening in southern Tibet: New age and geochemical constraints from the Gangdese batholith. *J. Asian Earth Sci.* **2012**, *53*, 82–95. [CrossRef]
7. Jiang, X.; Zhao, Z.D.; Zhu, D.C.; Zhang, F.Q.; Dong, G.C.; Mo, X.X.; Guo, T.Y. Zircon U-Pb geochronology and Hf isotopic geochemistry of Jiangba, Bangba, and Xiongba granitoids in western Gangdese, Tibet. *Acta Petrol. Sin.* **2010**, *26*, 2155–2164. (In Chinese with English Abstract)
8. Kapp, P.; DeCelles, P.G.; Gehrels, G.E.; Heizler, M.; Ding, L. Geological records of the Lhasa-Qiangtang and Indo-Asian collisions in the Nima area of central Tibet. *Geol. Soc. Am. Bull.* **2007**, *119*, 917–932. [CrossRef]
9. Wen, D.R.; Liu, D.Y.; Chung, S.L.; Chu, M.F.; Ji, J.Q.; Zhang, Q.; Song, B.; Lee, T.Y.; Yeh, M.W.; Lo, C.H. Zircon SHRIMP U–Pb ages of the Gangdese Batholith and implications for Neo-Tethyan subduction in southern Tibet. *Chem. Geol.* **2008**, *252*, 191–201. [CrossRef]
10. Chen, X.; Zheng, Y.Y.; Gao, S.B.; Wu, S.; Jiang, X.J.; Jiang, J.S.; Lin, C.G. Ages and petrogenesis of the late Triassic andesitic rocks at the Luerma porphyry Cu deposit, western Gangdese, and implications for regional metallogeny. *Gondwana Res.* **2020**, *85*, 103–123. [CrossRef]
11. Guo, L.; Liu, Y.; Liu, S.; Cawood, P.A.; Wang, Z.; Liu, H. Petrogenesis of Early to Middle Jurassic granitoid rocks from the Gangdese belt, Southern Tibet: Implications for early history of the Neo-Tethys. *Lithos* **2013**, *179*, 320–333. [CrossRef]
12. Kang, Z.Q.; Xu, J.F.; Simon, A.W.; Feng, Z.H.; Chen, J.L.; Wang, B.D.; Fu, W.C.; Pan, H.B. Geochronology and geochemistry of the Sangri group volcanic rocks, southern Lhasa Terrane: Implications for the early subduction history of the Neo-Tethys and Gangdese magmatic arc. *Lithos* **2014**, *200–201*, 157–168. [CrossRef]
13. Meng, Y.K.; Xu, Z.Q.; Chen, X.J.; Ma, X.X.; He, Z.Y.; Zhang, X.S. Zircon geochronology and Hf isotopic composition of Eocene granite batholith from Xaitongmoin in middle Gangdese and geological significance. *Geotecton. Metallog.* **2015**, *39*, 933–948. (In Chinese with English Abstract)
14. Wang, C.; Ding, L.; Zhang, L.Y.; Kapp, P.; Pullen, A.; Yue, Y.H. Petrogenesis of middle-late triassic volcanic rocks from the Gangdese belt, southern Lhasa terrane: Implications for early subduction of Neo-Tethyan oceanic lithosphere. *Lithos* **2016**, *262*, 320–333. [CrossRef]

15. Li, X.B.; Wang, B.D.; Liu, H.; Wang, L.Q.; Chen, L. The Late Jurassic high-Mg andesites in the Daru Tso area, Tibet: Evidence for the subduction of the Bangong Co-Nujiang River oceanic lithosphere. *Geol. Bull. China* **2015**, *34*, 251–261. (In Chinese with English Abstract)
16. Yan, J.J.; Zhao, Z.D.; Liu, D.; Wang, Z.Z.; Tang, Y. Geochemistry and petrogenesis of the Late Jurassic Xuru Tsobatholith in central Lhasa Terrane, Tibet. *Acta Petrol. Sin.* **2017**, *33*, 2437–2453. (In Chinese with English Abstract)
17. Meng, Y.K.; Xu, Z.Q.; Santosh, M.X.; Chen, X.J.; Guo, G.L.; Liu, F. Late Triassic crustal growth in southern Tibet: Evidence from the Gangdese magmatic belt. *Gondwana Res.* **2016**, *37*, 449–464. [CrossRef]
18. Lang, X.H.; Wang, X.H.; Deng, Y.L.; Tang, J.X.; Xie, F.W.; Zou, Y.; Huang, Y.; Li, Z.; Yin, Q.; Jiang, K. Early Jurassic volcanic rocks in the Xiongcun district, southern Lhasa subterrane, Tibet: Implications for the tectono-magmatic events associated with the early evolution of the Neo-Tethys Ocean. *Lithos* **2019**, *340–341*, 166–180. [CrossRef]
19. Ma, L.; Kerr, A.C.; Wang, Q.; Jiang, Z.Q.; Tang, G.J.; Yang, J.H.; Xia, X.; Hu, W.; Yang, Z.; Sun, P. Nature and Evolution of Crust in Southern Lhasa, Tibet: Transformation from Microcontinent to Juvenile Terrane. *J. Geophys. Res. Solid Earth* **2019**, *124*, 6452–6474. [CrossRef]
20. Hou, Z.Q.; Duan, L.F.; Lu, Y.J.; Zheng, Y.C.; Zhu, D.C.; Yang, Z.M.; Yang, Z.S.; Wang, B.D.; Pei, Y.R.; Zhao, Z.D.; et al. Lithospheric architecture of the Lhasa terrane and its control on ore deposits in the Himalayan-Tibetan Orogen. *Econ. Geol.* **2015**, *110*, 1541–1575. [CrossRef]
21. Jiang, J.S.; Zheng, Y.Y.; Gao, S.B.; Zhang, Y.C.; Huang, J.; Liu, J.; Wu, S.; Xu, J.; Huang, L.L. The newly-discovered Late Cretaceous igneous rocks in the Nuocang district: Products of ancient crust melting trigged by Neo-Tethyan slab rollback in the western Gangdese. *Lithos* **2018**, *308–309*, 294–315. [CrossRef]
22. Yin, A.; Harrison, T.M. Geologic evolution of the Himalayan–Tibetan orogen. *Annu. Rev. Earth Planet. Sci. Lett.* **2000**, *28*, 211–280. [CrossRef]
23. Lu, S.W.; Ren, J.D.; Bai, G.D.; Yang, J.F.; Lv, J.G. Discovery of the Mid-Late Jurassic Songmuguo strongly peraluminous granite belt in the southern part of Nyima County, Tibet, and its significance. *Geol. China* **2006**, *34*, 332–339. (In Chinese with English Abstract)
24. Zhang, H.F.; Xu, W.C.; Guo, J.Q.; Zong, K.Q.; Cai, H.M.; Yuan, H.L. Zircon U–Pb and Hf isotopic composition of deformed granite in the southern margin of the Gangdese belt, Tibet: Evidence for early Jurassic subduction of Neo-Tethyan oceanic slab. *Acta Petrol. Sin.* **2007**, *23*, 1347–1353. (In Chinese with English Abstract)
25. Zhang, L.L.; Liu, C.Z.; Wu, F.Y.; Ji, W.Q.; Wang, J.G. Zedong terrane revisited: An intra-oceanic arc within Neo-Tethys or a part of the Asian active continental margin? *J. Asian Earth Sci.* **2014**, *80*, 34–55. [CrossRef]
26. Zou, Y.Q.; Chen, X.L.; Huang, W.T.; Zhang, J.; Liang, H.Y.; Xu, J.F.; Chen, L. Identification of an Early–Middle Jurassic oxidized magmatic belt, south Gangdese, Tibet, and geological implications. *Sci. Bull.* **2017**, *62*, 888–898. [CrossRef]
27. Mo, X.X.; Hou, Z.Q.; Niu, Y.L.; Dong, G.C.; Qu, X.M.; Zhao, Z.D.; Yang, Z.M. Mantle contributions to crustal thickening during continental collision: Evidence from Cenozoic igneous rocks in southern Tibet. *Lithos* **2007**, *96*, 225–242. [CrossRef]
28. Mo, X.X.; Niu, Y.L.; Dong, G.C.; Zhao, Z.D.; Hou, Z.Q.; Zhou, S.; Ke, S. Contribution of syn-collisional felsic magmatism to continental crust growth: A case study of the Paleogene Linzizong volcanic succession in southern Tibet. *Chem. Geol.* **2008**, *250*, 49–67. [CrossRef]
29. Hou, Z.Q.; Gao, Y.F.; Qu, X.M.; Rui, Z.Y.; Mo, X.X. Origin of adakitic intrusives generated during mid-Miocene east–west extension in southern Tibet. *Earth Planet. Sci. Lett.* **2004**, *220*, 139–155. [CrossRef]
30. Wu, S.; Zheng, Y.Y.; Sun, X. Subduction metasomatism and collision-related metamorphic dehydration controls on the fertility of porphyry copper ore-forming high Sr/Y magma in Tibet. *Ore Geol. Rev.* **2016**, *73*, 83–103. [CrossRef]
31. Meng, Y.K.; Wang, Z.B.; Gan, B.P.; Liu, J.Q. Petrogenesis and tectonic implications of the Early Cretaceous granitic pluton in the Sulu orogenic belt: The Caochang granitic pluton as an example. *Minerals* **2020**, *10*, 432. [CrossRef]
32. Wei, Y.Q.; Zhao, Z.D.; Niu, Y.L.; Zhu, D.C.; Liu, D.; Wang, Q.; Hou, Z.Q.; Mo, X.X.; Wei, J.C. Geochronology and geochemistry of the Early Jurassic Yeba Formation volcanic rocks in southern Tibet: Initiation of back-arc rifting and crustal accretion in the southern Lhasa Terrane. *Lithos* **2017**, *278–281*, 477–490. [CrossRef]
33. Zhu, D.C.; Pan, G.T.; Wang, L.Q.; Mo, X.X.; Zhao, Z.D.; Zhou, C.Y.; Liao, Z.L.; Dong, G.C.; Yuan, S.H. Tempo-spatial variations of Mesozoicmagmatic rocks in the Gangdese belt, Tibet, China, with a discussion of geodynamic setting-related issues. *Geol. Bull. China* **2008**, *27*, 1535–1550. (In Chinese with English Abstract)
34. Zhu, D.C.; Zhao, Z.D.; Pan, G.T.; Lee, H.Y.; Kang, Z.Q.; Liao, Z.L.; Wang, L.Q.; Li, G.M.; Dong, G.C.; Liu, B. Early cretaceous subduction-related adakite-like rocks of the Gangdese Belt, southern Tibet: Products of slab melting and subsequent melt–peridotite interaction? *J. Asian Earth Sci.* **2009**, *34*, 298–309. [CrossRef]
35. Zhu, D.C.; Li, S.M.; Peter, A.; Wang, Q.; Zhao, Z.D.; Liu, S.A.; Wang, L.Q. Assembly of the Lhasa and Qiangtang terranes in central Tibet by divergent double subduction. *Lithos* **2016**, *245*, 7–17. [CrossRef]
36. Yao, S.; Li, P.; Guo, X.F.; Lu, X.J.; Zhang, X.T. Ore-forming geological characteristics and prospecting perspective analysis of the Magui lead-zinc polymetallic ore deposit in Tibet. *Geol. Bull. China* **2016**, *35*, 1529–15359. (In Chinese with English Abstract)
37. Liu, Y.S.; Hu, Z.C.; Gao, S.; Günther, D.; Xu, J.; Gao, C.G.; Chen, H.H. In situ analysis of major and trace elements of anhydrous minerals by LA-ICP-MS without applying an internal standard. *Chem. Geol.* **2008**, *257*, 34–43. [CrossRef]
38. Ludwig, K.R. *ISOPLOT 3.0: A Geochronological Toolkit for Microsoft Excel*; Berkeley Geochronology Center: Berkeley, CA, USA, 2003.
39. Fisher, C.M.; Vervoort, J.D.; Hanchar, J.M. Guidelines for reporting zircon Hf isotopic data by LA-MC-ICPMS and potential pitfalls in the interpretation of these data. *Chem. Geol.* **2014**, *363*, 125–133. [CrossRef]

40. Lin, J.; Liu, Y.S.; Yang, Y.H.; Hu, Z.C. Calibration and correction of LA-ICP-MS and LA-MC-ICP-MS analyses for element contents and isotopic ratios. *Solid Earth Sci.* **2016**, *1*, 5–27. [CrossRef]
41. Rudnick, R.L.; Gao, S. Composition of the continental crust. *Treatise Geochem.* **2003**, *3*, 21–64.
42. Defant, M.J.; Drummond, M.S. Derivation of some modern arc magmas by melting of young subducted lithosphere. *Nature* **1990**, *347*, 662–665. [CrossRef]
43. Middlemost, E.A.K. Naming materials in the magma/igneous rock system. *Earth Sci. Rev.* **1994**, *37*, 215–224. [CrossRef]
44. Peccerillo, A.; Taylor, S.R. Geochemistry of Eocene calc-alkaline volcanic rocks from the Kastamonu area, Northern Turkey. *Contrib. Mineral. Petrol.* **1976**, *58*, 63–81. [CrossRef]
45. Shand, S.J. *The Eruptive Rocks*; John Wiley & Sons, Inc.: New York, NY, USA, 1947; pp. 52–68.
46. Sun, S.S.; McDonough, W.F. Chemical and isotopic systematics of oceanic basalts: Implications for mantle composition and processes. *Geol. Soc. Lond. Spec. Publ.* **1989**, *42*, 313–345. [CrossRef]
47. Liu, M.; Zhao, Z.D.; Guan, Q.; Dong, G.C.; Mo, X.X.; Liu, Y.S.; Hu, Z.C. Tracing magma mixing genesis of the middle Early-Jurassic host granites and enclaves in Nyainrong microcontinent, Tibet from zircon LA-ICP-MS U-Pb dating and Hf isotopes. *Acta Petrol. Sin.* **2011**, *27*, 1931–1937. (In Chinese with English Abstract)
48. Collins, W.J.; Beams, S.D.; White, A.J.R. Nature and origin of A-type granites with particular reference to southeastern Australia. *Contrib. Mineral. Petrol.* **1982**, *80*, 189–200. [CrossRef]
49. Boehnke, P.; Watson, E.B.; Trail, D.; Harrison, T.M.; Schmitt, A.K. Zircon saturation re-revisited. *Chem. Geol.* **2013**, *351*, 324–334. [CrossRef]
50. Watson, E.B.; Harrison, T.M. Accessory minerals and the geochemical evolution of crustal magmatic systems: A summary and prospectus of experimental approaches. *Phys. Earth Planet. Inter.* **1984**, *35*, 19–30. [CrossRef]
51. King, P.L.; Chappell, B.W.; Allen, C.M.; White, A.J.R. Are A-type granites the high temperature felsic granites? Evidence from fractionated granites of the Wangrah Suite. *Aust. J. Earth Sci.* **2001**, *48*, 501–514. [CrossRef]
52. Chappell, B.W.; White, A.J.R. Two contrasting granite types: 25 years later. *Aust. J. Earth Sci.* **2001**, *48*, 489–499. [CrossRef]
53. Whalen, J.B.; Currie, K.L.; Chappell, B.W. A-type Granites: Geochemical Characteristics, Discrimination and Petrogenesis. *Contrib. Mineral. Petrol.* **1987**, *95*, 407–419. [CrossRef]
54. Hutchison, W.; Mather, T.A.; Pyle, D.M.; Boyce, A.J.; Gleeson, M.L.M.; Yirgu, G.; Blundy, J.D.; Ferguson, D.J.; Vye-Brown, C.; Millar, I.L.; et al. The evolution of magma during continental rifting: New constraints from the isotopic and trace element signatures of silicic magmas from Ethiopian volcanoes. *Earth Planet. Sci. Lett.* **2018**, *489*, 203–218. [CrossRef]
55. Soesoo, A. Fractional crystallization of mantle-derived melts as a mechanism for some I-type granite petrogenesis: An example from Lachlan Fold Belt. *Aust. J. Earth Sci.* **2000**, *157*, 135–149. [CrossRef]
56. Kemp, A.I.S.; Hawkesworth, C.J.; Foster, G.L.; Paterson, B.A.; Woodhead, J.D.; Hergt, J.M.; Gray, C.M.; Whitehouse, M.J. Magmatic and crustal differentiation history of granitic rocks from Hf–O isotopes in zircon. *Science* **2007**, *315*, 980–983. [CrossRef]
57. Foland, K.A.; Allen, J.C. Magma sources for Mesozoic anorogenic granites of the White Mountain magma series, New England, USA. *Contrib. Mineral. Petrol.* **1991**, *109*, 195–211. [CrossRef]
58. Frost, C.D.; Frost, B.R.; Chamberlain, K.R.; Edwards, B.R. Petrogenesis of the 1.43 Ga Sherman batholith, SE Wyoming, USA: A reduced, rapakivi-type anorogenic granite. *J. Petrol.* **1999**, *40*, 1771–1802. [CrossRef]
59. Altherr, R.; Holl, A.; Hegner, E.; Langer, C.; Kreuzer, H. High-potassium, calc-alkaline I-type plutonism in the European Variscides: Northern Vosges (France) and northern Schwarzwald (Germany). *Lithos* **2000**, *50*, 51–73. [CrossRef]
60. Hou, Z.Q.; Yang, Z.M.; Lu, Y.J.; Kemp, A.; Zheng, Y.C.; Li, Q.Y.; Tang, J.X.; Yang, Z.S.; Duan, L.F. A genetic linkage between subduction-and collision-related porphyry Cu deposits in continental collision zones. *Geology* **2015**, *43*, 247–250. [CrossRef]
61. Dewey, J.F.; Shackelton, R.M.; Chang, C.F.; Sun, Y.Y. The tectonic evolution of the Tibetan plateau. Philosophical transactions—Royal Society. *Biol. Sci.* **1988**, *327*, 379–413.
62. Garzanti, E.; Le Fort, P.; Sciunnach, D. First report of Lower Permian basalts in South Tibet: Tholeiitic magmatism during break-up and incipient opening of Neotethys. *J. Asian Earth Sci.* **1999**, *17*, 533–546. [CrossRef]
63. Sciunnach, D.; Garzanti, E. Subsidence history of the Tethys Himalaya. *Earth-Sci. Rev.* **2012**, *111*, 179–198. [CrossRef]
64. Zhu, D.C.; Zhao, Z.D.; Niu, Y.; Dilek, Y.; Hou, Z.Q.; Mo, X.X. The origin and pre-Cenozoic evolution of the Tibetan Plateau. *Gondwana Res.* **2013**, *23*, 1429–1454. [CrossRef]
65. Ding, L.; Xu, Q.; Yue, Y.; Wang, H.; Cai, F.; Li, S. The Andean-type Gangdese Mountains: Paleoelevation record from the Paleocene–Eocene Linzhou Basin. *Earth Planet. Sci. Lett.* **2014**, *392*, 250–264. [CrossRef]
66. Song, S.W.; Liu, Z.; Zhu, D.C.; Wang, Q.; Zhang, L.X.; Zhang, L.L.; Zhao, Z.D. Zircon U-Pb chronology and Hf isotope of the Late Triassic andesitic magmatism in Dajiacuo, Tibet. *Acta Petrol. Sin.* **2014**, *30*, 3100–3112. (In Chinese with English Abstract)
67. Coulon, C.; Maluski, H.; Bollonger, C.; Wang, S. Mesozoic and Cenozoic volcanic rocks from central and southern Tibet: 39Ar–40Ar dating, petrological characteristics and geodynamical significance. *Earth Planet. Sci. Lett.* **1986**, *79*, 281–302. [CrossRef]
68. Pearce, J.A.; Peate, D.W. Tectonic implications of the composition of volcanic arc magmas. *Annu. Rev. Earth Planet. Sci.* **1995**, *23*, 251–285. [CrossRef]
69. Pearce, J.A.; Harris, N.B.W.; Tindle, A.G. Trace Element Discrimination Diagrams for the Tectonic Interpretation of Granitic Rocks. *J. Petrol.* **1984**, *25*, 956–983. [CrossRef]
70. Gorton, M.P.; Schandl, E.S. From continents to islands arcs: A geochemical index of tectonics setting for arc-related and within-plate felsic to intermediate volcanics rocks. *Can. Mineral.* **2000**, *38*, 1065–1073. [CrossRef]